Featured in Physics

Observation of the Electromagnetic Field Effect via Charge-Dependent Directed Flow in Heavy-Ion Collisions at the Relativistic Heavy Ion Collider

M. I. Abdulhamid,[4] B. E. Aboona,[55] J. Adam,[15] J. R. Adams,[40] G. Agakishiev,[30] I. Aggarwal,[41] M. M. Aggarwal,[41] Z. Ahammed,[61] A. Aitbaev,[30] I. Alekseev,[2,37] E. Alpatov,[37] A. Aparin,[30] S. Aslam,[26] J. Atchison,[1] G. S. Averichev,[30] V. Bairathi,[53] J. G. Ball Cap,[22] K. Barish,[11] P. Bhagat,[29] A. Bhasin,[29] S. Bhatta,[52] S. R. Bhosale,[17] I. G. Bordyuzhin,[2] J. D. Brandenburg,[40] A. V. Brandin,[37] X. Z. Cai,[50] H. Caines,[64] M. Calderón de la Barca Sánchez,[9] D. Cebra,[9] J. Ceska,[15] I. Chakaberia,[33] B. K. Chan,[10] Z. Chang,[27] A. Chatterjee,[16] D. Chen,[11] J. Chen,[49] J. H. Chen,[19] Z. Chen,[49] J. Cheng,[57] Y. Cheng,[10] S. Choudhury,[19] W. Christie,[6] X. Chu,[6] H. J. Crawford,[8] G. Dale-Gau,[13] A. Das,[15] A. P. Dash,[10] M. Daugherity,[1] T. G. Dedovich,[30] I. M. Deppner,[21] A. A. Derevschikov,[42] A. Dhamija,[41] P. Dixit,[24] X. Dong,[33] J. L. Drachenberg,[1] E. Duckworth,[31] J. C. Dunlop,[6] J. Engelage,[8] G. Eppley,[44] S. Esumi,[58] O. Evdokimov,[13] O. Eyser,[6] R. Fatemi,[32] S. Fazio,[7] C. J. Feng,[39] Y. Feng,[43] E. Finch,[51] Y. Fisyak,[6] F. A. Flor,[64] C. Fu,[28] T. Gao,[49] F. Geurts,[44] N. Ghimire,[54] A. Gibson,[60] K. Gopal,[25] X. Gou,[49] D. Grosnick,[60] A. Gupta,[29] A. Hamed,[4] Y. Han,[44] M. D. Harasty,[9] J. W. Harris,[64] H. Harrison-Smith,[32] W. He,[19] X. H. He,[28] Y. He,[49] C. Hu,[59] Q. Hu,[28] Y. Hu,[33] H. Huang,[39] H. Z. Huang,[10] S. L. Huang,[52] T. Huang,[13] X. Huang,[57] Y. Huang,[57] Y. Huang,[12] T. J. Humanic,[40] D. Isenhower,[1] M. Isshiki,[58] W. W. Jacobs,[27] A. Jalotra,[29] C. Jena,[25] Y. Ji,[33] J. Jia,[6,52] C. Jin,[44] X. Ju,[46] E. G. Judd,[8] S. Kabana,[53] D. Kalinkin,[32] K. Kang,[57] D. Kapukchyan,[11] K. Kauder,[6] D. Keane,[31] A. Kechechyan,[30] A. Kiselev,[6] A. G. Knospe,[34] H. S. Ko,[33] L. Kochenda,[37] A. A. Korobitsin,[30] A. Yu. Kraeva,[37] P. Kravtsov,[37] L. Kumar,[41] M. C. Labonte,[9] R. Lacey,[52] J. M. Landgraf,[6] A. Lebedev,[6] R. Lednicky,[30] J. H. Lee,[6] Y. H. Leung,[21] N. Lewis,[6] C. Li,[49] H-S. Li,[43] W. Li,[44] X. Li,[46] Y. Li,[46] Y. Li,[57] Z. Li,[46] X. Liang,[11] Y. Liang,[31] T. Lin,[49] Y. Lin,[20] C. Liu,[28] F. Liu,[12] G. Liu,[47] H. Liu,[12] L. Liu,[12] T. Liu,[64] X. Liu,[40] Y. Liu,[55] Z. Liu,[12] T. Ljubicic,[6] O. Lomicky,[15] R. S. Longacre,[6] E. M. Loyd,[11] T. Lu,[28] N. S. Lukow,[54] X. F. Luo,[12] V. B. Luong,[30] L. Ma,[19] R. Ma,[6] Y. G. Ma,[19] N. Magdy,[52] D. Mallick,[62] S. Margetis,[31] H. S. Matis,[33] G. McNamara,[63] K. Mi,[12] N. G. Minaev,[42] B. Mohanty,[38] M. M. Mondal,[38] I. Mooney,[64] D. A. Morozov,[42] A. Mudrokh,[30] M. I. Nagy,[17] A. S. Nain,[41] J. D. Nam,[54] M. Nasim,[24] E. Nedorezov,[30] D. Neff,[10] J. M. Nelson,[8] D. B. Nemes,[64] M. Nie,[49] G. Nigmatkulov,[13] T. Niida,[58] L. V. Nogach,[42] T. Nonaka,[58] G. Odyniec,[33] A. Ogawa,[6] S. Oh,[48] V. A. Okorokov,[37] K. Okubo,[58] B. S. Page,[6] R. Pak,[6] A. Pandav,[33] Y. Panebratsev,[30] T. Pani,[45] P. Parfenov,[37] A. Paul,[11] C. Perkins,[8] B. R. Pokhrel,[54] M. Posik,[54] A. Povarov,[37] T. Protzman,[34] N. K. Pruthi,[41] J. Putschke,[63] Z. Qin,[57] H. Qiu,[28] A. Quintero,[54] C. Racz,[11] S. K. Radhakrishnan,[31] A. Rana,[41] R. L. Ray,[56] H. G. Ritter,[33] C. W. Robertson,[43] O. V. Rogachevsky,[30] M. A. Rosales Aguilar,[32] D. Roy,[45] L. Ruan,[6] A. K. Sahoo,[24] N. R. Sahoo,[25] H. Sako,[58] S. Salur,[45] E. Samigullin,[2] S. Sato,[58] B. C. Schaefer,[34] W. B. Schmidke,[6,*] N. Schmitz,[35] J. Seger,[14] R. Seto,[11] P. Seyboth,[35] N. Shah,[26] E. Shahaliev,[30] P. V. Shanmuganathan,[6] T. Shao,[19] M. Sharma,[29] N. Sharma,[24] R. Sharma,[25] S. R. Sharma,[25] A. I. Sheikh,[31] D. Shen,[49] D. Y. Shen,[19] K. Shen,[46] S. S. Shi,[12] Y. Shi,[49] Q. Y. Shou,[19] F. Si,[46] J. Singh,[41] S. Singha,[28] P. Sinha,[25] M. J. Skoby,[5,43] Y. Söhngen,[21] Y. Song,[64] B. Srivastava,[43] T. D. S. Stanislaus,[60] D. J. Stewart,[63] M. Strikhanov,[37] B. Stringfellow,[43] Y. Su,[46] C. Sun,[52] X. Sun,[28] Y. Sun,[46] Y. Sun,[23] B. Surrow,[54] D. N. Svirida,[2] Z. W. Sweger,[9] A. C. Tamis,[64] A. H. Tang,[6] Z. Tang,[46] A. Taranenko,[37] T. Tarnowsky,[36] J. H. Thomas,[33] D. Tlusty,[14] T. Todoroki,[58] M. V. Tokarev,[30] S. Trentalange,[10] P. Tribedy,[6] S. K. Tripathy,[62] O. D. Tsai,[10,6] C. Y. Tsang,[31,6] Z. Tu,[6] J. Tyler,[55] T. Ullrich,[6] D. G. Underwood,[3,60] I. Upsal,[46] G. Van Buren,[6] A. N. Vasiliev,[42,37] V. Verkest,[63] F. Videbæk,[6] S. Vokal,[30] S. A. Voloshin,[63] F. Wang,[43] G. Wang,[10] J. S. Wang,[23] J. Wang,[49] X. Wang,[49] Y. Wang,[46] Y. Wang,[12] Y. Wang,[57] Z. Wang,[49] J. C. Webb,[6] P. C. Weidenkaff,[21] G. D. Westfall,[36] H. Wieman,[33] G. Wilks,[13] S. W. Wissink,[27] J. Wu,[12] J. Wu,[28] X. Wu,[10] X. Wu,[46] B. Xi,[19] Z. G. Xiao,[57] G. Xie,[59] W. Xie,[43] H. Xu,[23] N. Xu,[33] Q. H. Xu,[49] Y. Xu,[49] Y. Xu,[12] Z. Xu,[31] Z. Xu,[10] G. Yan,[49] Z. Yan,[52] C. Yang,[49] Q. Yang,[49] S. Yang,[47] Y. Yang,[39] Z. Ye,[44] Z. Ye,[33] L. Yi,[49] K. Yip,[6] Y. Yu,[49] W. Zha,[46] C. Zhang,[19] D. Zhang,[47] J. Zhang,[49] S. Zhang,[46] W. Zhang,[47] X. Zhang,[28] Y. Zhang,[28] Y. Zhang,[46] Y. Zhang,[49] Y. Zhang,[12] Z. J. Zhang,[39] Z. Zhang,[6] Z. Zhang,[13] F. Zhao,[28] J. Zhao,[19] M. Zhao,[6] C. Zhou,[19] J. Zhou,[46] S. Zhou,[12] Y. Zhou,[12] X. Zhu,[57] M. Zurek,[3,6] and M. Zyzak[18]

(STAR Collaboration)

[1]*Abilene Christian University, Abilene, Texas 79699*
[2]*Alikhanov Institute for Theoretical and Experimental Physics NRC "Kurchatov Institute," Moscow 117218*
[3]*Argonne National Laboratory, Argonne, Illinois 60439*
[4]*American University in Cairo, New Cairo 11835, Egypt*
[5]*Ball State University, Muncie, Indiana, 47306*

[6]Brookhaven National Laboratory, Upton, New York 11973
[7]University of Calabria and INFN-Cosenza, Rende 87036, Italy
[8]University of California, Berkeley, California 94720
[9]University of California, Davis, California 95616
[10]University of California, Los Angeles, California 90095
[11]University of California, Riverside, California 92521
[12]Central China Normal University, Wuhan, Hubei 430079
[13]University of Illinois at Chicago, Chicago, Illinois 60607
[14]Creighton University, Omaha, Nebraska 68178
[15]Czech Technical University in Prague, FNSPE, Prague 115 19, Czech Republic
[16]National Institute of Technology Durgapur, Durgapur-713209, India
[17]ELTE Eötvös Loránd University, Budapest, Hungary H-1117
[18]Frankfurt Institute for Advanced Studies FIAS, Frankfurt 60438, Germany
[19]Fudan University, Shanghai, 200433
[20]Guangxi Normal University, Guilin
[21]University of Heidelberg, Heidelberg 69120, Germany
[22]University of Houston, Houston, Texas 77204
[23]Huzhou University, Huzhou, Zhejiang 313000
[24]Indian Institute of Science Education and Research (IISER), Berhampur 760010, India
[25]Indian Institute of Science Education and Research (IISER) Tirupati, Tirupati 517507, India
[26]Indian Institute Technology, Patna, Bihar 801106, India
[27]Indiana University, Bloomington, Indiana 47408
[28]Institute of Modern Physics, Chinese Academy of Sciences, Lanzhou, Gansu 730000
[29]University of Jammu, Jammu 180001, India
[30]Joint Institute for Nuclear Research, Dubna 141 980
[31]Kent State University, Kent, Ohio 44242
[32]University of Kentucky, Lexington, Kentucky 40506-0055
[33]Lawrence Berkeley National Laboratory, Berkeley, California 94720
[34]Lehigh University, Bethlehem, Pennsylvania 18015
[35]Max-Planck-Institut für Physik, Munich 80805, Germany
[36]Michigan State University, East Lansing, Michigan 48824
[37]National Research Nuclear University MEPhI, Moscow 115409
[38]National Institute of Science Education and Research, HBNI, Jatni 752050, India
[39]National Cheng Kung University, Tainan 70101
[40]The Ohio State University, Columbus, Ohio 43210
[41]Panjab University, Chandigarh 160014, India
[42]NRC "Kurchatov Institute," Institute of High Energy Physics, Protvino 142281
[43]Purdue University, West Lafayette, Indiana 47907
[44]Rice University, Houston, Texas 77251
[45]Rutgers University, Piscataway, New Jersey 08854
[46]University of Science and Technology of China, Hefei, Anhui 230026
[47]South China Normal University, Guangzhou, Guangdong 510631
[48]Sejong University, Seoul, 05006, South Korea
[49]Shandong University, Qingdao, Shandong 266237
[50]Shanghai Institute of Applied Physics, Chinese Academy of Sciences, Shanghai 201800
[51]Southern Connecticut State University, New Haven, Connecticut 06515
[52]State University of New York, Stony Brook, New York 11794
[53]Instituto de Alta Investigación, Universidad de Tarapacá, Arica 1000000, Chile
[54]Temple University, Philadelphia, Pennsylvania 19122
[55]Texas A&M University, College Station, Texas 77843
[56]University of Texas, Austin, Texas 78712
[57]Tsinghua University, Beijing 100084
[58]University of Tsukuba, Tsukuba, Ibaraki 305-8571, Japan
[59]University of Chinese Academy of Sciences, Beijing, 101408
[60]Valparaiso University, Valparaiso, Indiana 46383
[61]Variable Energy Cyclotron Centre, Kolkata 700064, India

[62]*Warsaw University of Technology, Warsaw 00-661, Poland*
[63]*Wayne State University, Detroit, Michigan 48201*
[64]*Yale University, New Haven, Connecticut 06520*

(Received 10 April 2023; revised 14 December 2023; accepted 11 January 2024; published 23 February 2024)

The deconfined quark-gluon plasma (QGP) created in relativistic heavy-ion collisions enables the exploration of the fundamental properties of matter under extreme conditions. Noncentral collisions can produce strong magnetic fields on the order of 10^{18} G, which offers a probe into the electrical conductivity of the QGP. In particular, quarks and antiquarks carry opposite charges and receive contrary electromagnetic forces that alter their momenta. This phenomenon can be manifested in the collective motion of final-state particles, specifically in the rapidity-odd directed flow, denoted as $v_1(\mathsf{y})$. Here, we present the charge-dependent measurements of $dv_1/d\mathsf{y}$ near midrapidities for $\pi^{\pm}$, $K^{\pm}$, and $p(\bar{p})$ in Au + Au and isobar ($^{96}_{44}\text{Ru}+^{96}_{44}\text{Ru}$ and $^{96}_{40}\text{Zr}+^{96}_{40}\text{Zr}$) collisions at $\sqrt{s_{\text{NN}}}=200$ GeV, and in Au + Au collisions at 27 GeV, recorded by the STAR detector at the Relativistic Heavy Ion Collider. The combined dependence of the v_1 signal on collision system, particle species, and collision centrality can be qualitatively and semiquantitatively understood as several effects on constituent quarks. While the results in central events can be explained by the *u* and *d* quarks transported from initial-state nuclei, those in peripheral events reveal the impacts of the electromagnetic field on the QGP. Our data put valuable constraints on the electrical conductivity of the QGP in theoretical calculations.

DOI: 10.1103/PhysRevX.14.011028 Subject Areas: Nuclear Physics, Particles and Fields

I. INTRODUCTION

By colliding two heavy nuclei at high center-of-mass energies ($\sqrt{s_{\text{NN}}}$), experiments at the Brookhaven National Laboratory (BNL) Relativistic Heavy Ion Collider (RHIC) and the CERN Large Hadron Collider (LHC) can create a medium of liberated quarks and gluons, a state of matter known as the quark-gluon plasma (QGP) [1]. The QGP dominated the early Universe about a microsecond after the big bang [2], and its recreation in the laboratory provides a unique opportunity to study the fundamental properties of matter under extreme conditions. In these ultrarelativistic collisions, the nuclear fragments pass by each other, generating very strong magnetic fields, on the order of 10^{18} G [3–9], the evolution of which, in the presence of a QGP, must be described in conjunction with the QGP's electromagnetic properties. The presence of a strong magnetic field also facilitates the study of some novel phenomena related to the restoration of fundamental symmetries of quantum chromodynamics (QCD) [6,10–15]. For example, the chiral magnetic effect (CME) predicts a charge separation along the direction of the magnetic field due to the chirality imbalance and chiral symmetry restoration in the QGP [16–18]. If confirmed, the CME in heavy-ion collisions will uncover the local parity and charge-parity violation in the strong interaction [6]. The strong magnetic field could also interact with the QCD matter in other ways, such as providing a catalyst for chiral symmetry breaking [19], causing the synchrotron radiation from quarks [20], differentiating the chiral and deconfinement phase transitions in the QCD phase diagram [21], and modifying the collectivity of a QGP [22–28].

Direct evidence of the electromagnetic field in the QGP is elusive, because the magnetic field magnitude drops rapidly with time in the vacuum until the QCD medium is formed, after which the field couples with the induced electric current in the QGP. Previously, the Coulomb effect in asymmetric Cu + Au collisions was observed via charge-dependent rapidity-even directed flow, $v_1^{\text{even}}(\mathsf{y})$ [29,30]. Directed flow (v_1) is defined as the first Fourier coefficient of the particle azimuthal distribution relative to the reaction plane (the x-z plane in Fig. 1) [31,32]:

$$E\frac{d^3N}{d^3p}=\frac{1}{2\pi}\frac{d^2N}{p_T dp_T d\mathsf{y}}\left(1+\sum_{n=1}^{\infty}2v_n\cos n(\phi-\Psi)\right), \quad (1)$$

where $p_T=\sqrt{p_x^2+p_y^2}$ is transverse momentum while ϕ and Ψ are the azimuthal angles of a particle and the reaction plane, respectively. Note that rapidity (y) and p_z bear the same sign. $v_1(\mathsf{y})$ can be uniquely expressed as a combination of two components: an even function of y and an odd function. Recent studies suggest that the charge-dependent $v_1^{\text{odd}}(\mathsf{y})$ can serve as a probe to the electromagnetic field in symmetric heavy-ion collisions [24,26–28]; we explore this approach below. Hereafter, $v_1(\mathsf{y})$ implicitly refers to the odd component, which comes from the initial tilt of the

*Deceased.

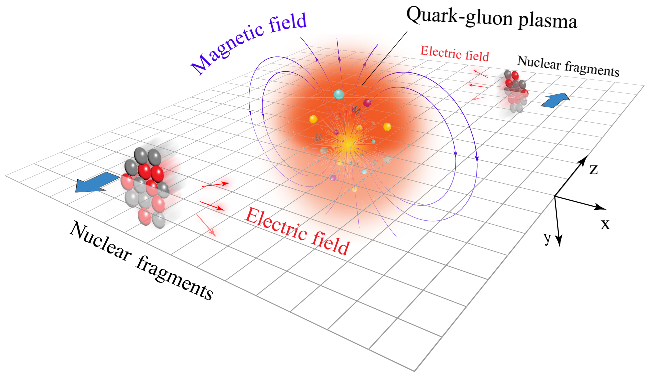

FIG. 1. Sketch of a heavy-ion collision in the lab frame. The impact parameter and the beam direction are along the x and z axes, respectively. The x-z plane is called the reaction plane. Participating nucleons in the overlap region create a hot and dense medium of quark-gluon plasma. Spectator nuclear fragments generate strong electromagnetic fields.

QGP (Fig. 2) and is sensitive to the equation of state [33,34]. Measurements of v_1 have been extensively performed over past decades at both RHIC and the LHC experiments [29,35–43]. It is common practice to present $dv_1/d\mathrm{y}$ because of the linear y dependence of v_1 near midrapidities in those experiments.

Figure 2 illustrates the overhead view of a heavy-ion collision, where the longitudinal expansion of the QGP has the same effect on v_1 for quarks with opposite charges. This degeneracy will be lifted by electromagnetic effects.

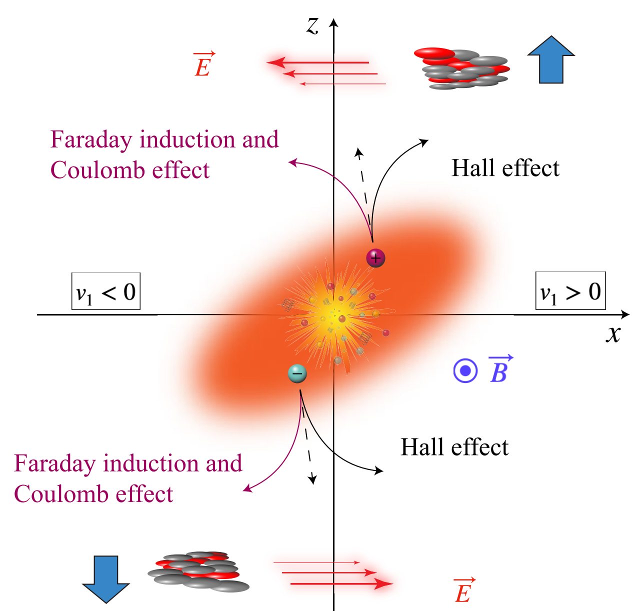

FIG. 2. Schematic overhead view (along the y axis) of a heavy-ion collision in the lab frame. The dashed lines represent the motion of quarks due to the QGP expansion. The black (purplish red) curved lines suggest the paths that quarks would follow due to the Lorentz force (Coulomb and Faraday field) alone.

For a positively charged quark, the Lorentz force in the Hall effect (black solid lines in Fig. 2) increases its v_1 at $\mathrm{y} > 0$ and decreases its v_1 at $\mathrm{y} < 0$, namely, increasing its $dv_1/d\mathrm{y}$. For a negatively charged quark, the Hall effect does the opposite and decreases its $dv_1/d\mathrm{y}$, contributing a positive $\Delta(dv_1/d\mathrm{y})$ [44]. In addition, the fast decay of the magnetic field in the QGP will induce an electric field, known as the Faraday induction effect, which, together with the electric field from spectator protons, renders a negative $\Delta(dv_1/d\mathrm{y})$ for quarks (purplish red lines). Theoretical calculations predict that the Faraday induction + Coulomb effect will dominate over the Hall effect on light quarks [26–28], and their roles are reversed on charm quarks that have relatively early formation time and long relaxation time [24]. The net effect for quarks will be translated into a finite $\Delta(dv_1/d\mathrm{y})$ between positively and negatively charged hadrons through quark coalescence. In the coalescence picture, the v_n of the resulting mesons or baryons is roughly equal to the summed v_n of their constituent quarks [40,45–47].

As a well-recognized paradigm, constituent quarks refer to valence quarks enveloped by a cloud of sea quarks and gluons, effectively gaining an enhanced mass. Mounting evidence supports the coalescence of two or three constituent quarks within the dense QGP medium, forming mesons or baryons. Although not understood at a fundamental level, this mechanism has demonstrated remarkable success in elucidating the multiplicity dependence of yields, spectra, and collective motions in heavy-ion collisions [40,45–50]. In this paper, we differentiate between two sources of constituent quarks: those generated as $q\bar{q}$ pairs and those transported from the initial-state nuclei to midrapidities. Transported quarks convey information from the incident nucleons and undergo the entire system evolution. Conversely, produced quarks are likely to form at various stages. In the high-$\sqrt{s_{\mathrm{NN}}}$ limit, most u and d quarks are produced, whereas in the low-$\sqrt{s_{\mathrm{NN}}}$ limit, most of them are presumably transported. The fraction of transported $u(d)$ in all $u(d)$ quarks can be estimated, e.g., following Boltzmann statistics with the experimentally measured temperature and baryon chemical potential of the collision system [47].

Experimental efforts have been made to search for the electromagnetic field effect in symmetric collisions, such as the $dv_1/d\mathrm{y}$ measurements for D^0 and $\bar{D}^0$ in Au + Au collisions at $\sqrt{s_{\mathrm{NN}}} = 200$ GeV by the STAR experiment [41]. In addition, the ALICE Collaboration has conducted similar measurements for charged hadrons and D^0 mesons in Pb + Pb collisions at $\sqrt{s_{\mathrm{NN}}} = 5.02$ TeV [51]. While the $\Delta(dv_1/d\mathrm{y})$ results for D^0 mesons are limited in significance by lack of statistics, those for charged hadrons (consisting mostly of light quarks) in 10%–40% centrality show positive values [41,51], which contradicts the theoretical expectation for the Faraday induction + Coulomb effect. Positive $\Delta(dv_1/d\mathrm{y})$ values between protons and

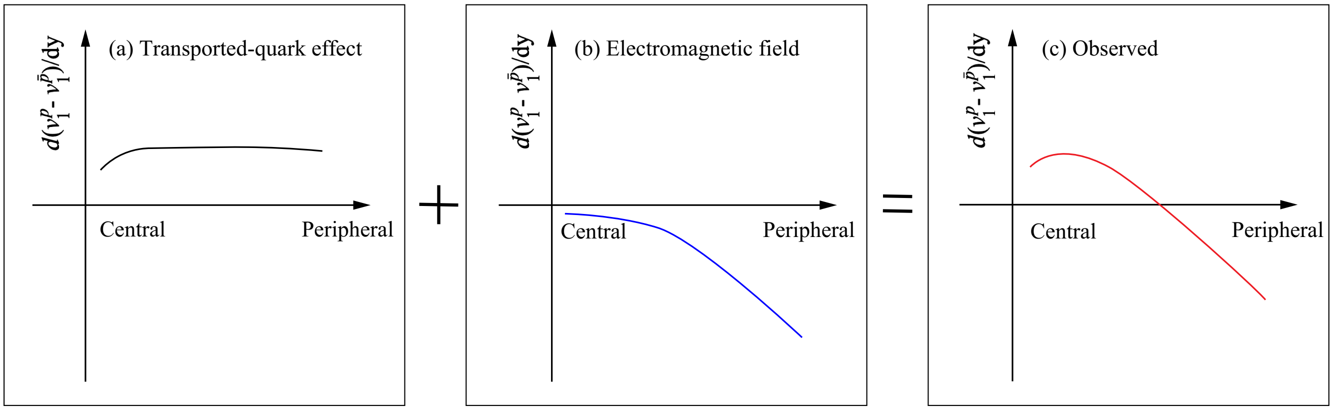

FIG. 3. Illustration of different contributions to the proton $\Delta(dv_1/dy)$ versus centrality. (a) depicts the transported-quark effect. (b) sketches the electromagnetic field contribution, dominated by the Faraday induction + Coulomb effect. (c) speculates the superposition of the two effects in the final observable.

antiprotons have also been obtained in semicentral Au + Au collisions at several RHIC energies [39,40] and are attributed to transported quarks. The transported u and d quarks acquire different azimuthal anisotropy than the pair-produced quarks in later stages, and they contribute to protons (uud) but not antiprotons ($\bar{u}\bar{u}\bar{d}$). Calculations from ultra relativistic quantum molecular dynamics (UrQMD) model [52], A multi-phase transport model [53], and a hydrodynamic model with an expanding fireball of inhomogeneous baryons [54] indicate that transported quarks have positive dv_1/dy and, hence, should give a positive contribution to $\Delta(dv_1/dy)$ between protons and antiprotons, as demonstrated in Fig. 3(a). A similar effect in the elliptic flow (v_2) difference between protons and antiprotons has also been observed in the RHIC beam energy scan (BES) data [46,47]. On the other hand, Fig. 3(b) shows the qualitative trend of the electromagnetic field effect on the proton $\Delta(dv_1/dy)$, in view of the more spectator protons in more peripheral collisions. If the Faraday induction + Coulomb effect dominates over the Hall effect and the transported-quark effect in peripheral collisions, a sign change of the proton $\Delta(dv_1/dy)$ could occur from positive in central events to negative in peripheral ones, as illustrated in Fig. 3(c). Therefore, the negative $\Delta(dv_1/dy)$ between protons and antiprotons can serve as a signature of the Faraday induction + Coulomb effect.

Similar to p and $\bar{p}$ in Fig. 3, the $\Delta(dv_1/dy)$ between K^+ and K^- could also change sign as a function of centrality, since transported u quarks increase the dv_1/dy for only $K^+(u\bar{s})$ but not $K^-(\bar{u}s)$, giving a positive contribution to the kaon $\Delta(dv_1/dy)$, while the electromagnetic field plays an opposite role that grows stronger in more peripheral events. Both $\pi^+(u\bar{d})$ and $\pi^-(\bar{u}d)$ are affected by transported quarks. Since the gold ion ($^{197}_{79}$Au) is neutron (udd) rich, there are more d quarks than u quarks transported in Au + Au collisions, and, thus, π^- is more influenced than π^+ [46], leading to a negative contribution to the $\Delta(dv_1/dy)$ between π^+ and π^-. As a side note, the v_2 difference between π^+ and π^- in the BES data has been quantitatively explained by the transported-quark effect [47,55]. Thus, the transported-quark effect and the Faraday induction + Coulomb effect work in the same direction for the pion $\Delta(dv_1/dy)$ and cannot be distinguished. In this work, we report the dv_1/dy measurements for $\pi^{\pm}$, $K^{\pm}$, and $p(\bar{p})$ in Au + Au collisions at $\sqrt{s_{\rm NN}} = 27$ and 200 GeV, and in isobar ($^{96}_{44}$Ru + $^{96}_{44}$Ru and $^{96}_{40}$Zr + $^{96}_{40}$Zr) collisions at 200 GeV, with the expectation that the large datasets may reveal a sign change in the proton and kaon $\Delta(dv_1/dy)$ as a function of centrality.

II. EXPERIMENT AND METHODOLOGY

The STAR experiment collected large data samples of minimum-bias-trigger events of Au + Au collisions at $\sqrt{s_{\rm NN}} = 200$ GeV in 2014 and 2016 and of isobar collisions at $\sqrt{s_{\rm NN}} = 200$ GeV and Au + Au collisions at $\sqrt{s_{\rm NN}} = 27$ GeV in 2018. The time projection chamber (TPC) [56] is used for charged particle tracking within pseudorapidity $|\eta| < 1$, with full 2π azimuthal coverage. For each event, the primary vertex position along the beam direction (the z axis) is reconstructed with both the TPC ($V_{z,\rm TPC}$) and the vertex position detectors ($V_{z,\rm VPD}$) [57]. The radial distance between the primary vertex and the z axis (V_r) is evaluated with the TPC. To ensure the event quality, each event is required to have a vertex position within $|V_{z,\rm TPC}| < 30$ cm (< 70 cm), $V_r < 2$ cm, and $|V_{z,\rm TPC} - V_{z,\rm VPD}| < 3$ cm (< 4 cm) for Au + Au collisions at 200 GeV (27 GeV) and within $-35 < V_{z,\rm TPC} < 25$ cm, $V_r < 2$ cm, and $|V_{z,\rm TPC} - V_{z,\rm VPD}| < 5$ cm for isobar collisions at 200 GeV. The asymmetric $V_{z,\rm TPC}$ cuts come from a negative mean value of $\langle V_{z,\rm TPC}\rangle = -5$ cm in isobar collisions. After the vertex selection, we have about 2.2 billion Au + Au events at 200 GeV, 400 million Au + Au events at 27 GeV, 1.7 billion Ru + Ru events, and 1.8 billion Zr + Zr events at 200 GeV. Centrality is defined by matching the distribution of the number of charged particles (detected by

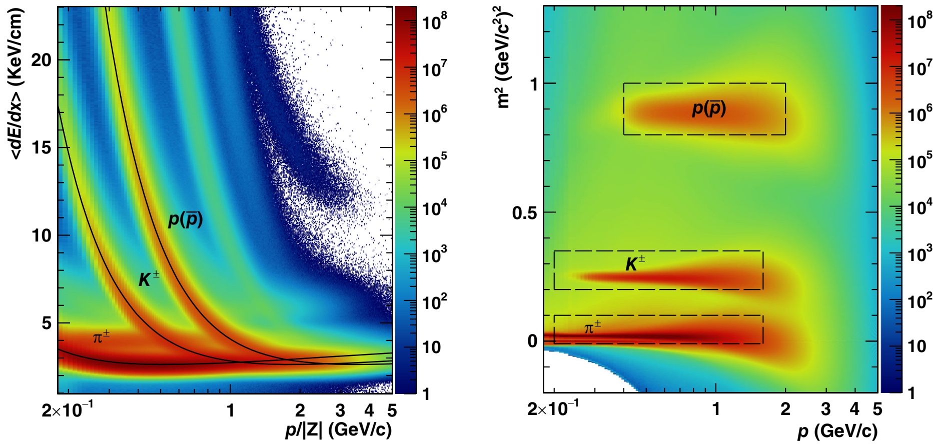

FIG. 4. Left: ionization energy loss ($\langle dE/dx \rangle$) of charged particles in the TPC versus magnetic rigidity in Au + Au collisions at $\sqrt{s_{NN}} = 200$ GeV. Solid lines denote the Bichsel functions. Right: mass squared (m^2) from the TOF versus momentum. Dashed boxes indicate the selection criteria for pions, kaons, and protons.

the TPC within $|\eta| < 0.5$) and the one obtained from MC Glauber simulations [58–60]. We focus on the centrality range of 0%–80%, where 0 refers to head-on collisions and 80% represents very peripheral collisions.

In this analysis, tracks within the TPC acceptance are required to have at least 15 space points (N_{hits}) and a distance of closest approach (DCA) to the primary vertex less than 2 cm in Au + Au collisions and less than 3 cm in isobar collisions. $\pi^{\pm}$, $K^{\pm}$, p, and $\bar{p}$ are identified based on the truncated mean value of the track energy loss ($\langle dE/dx \rangle$) in the TPC and time-of-flight (TOF) information from the TOF detector [61]. Figure 4 (left) presents an example of $\langle dE/dx \rangle$ versus magnetic rigidity for charged particles in Au + Au collisions at $\sqrt{s_{NN}} = 200$ GeV. Pions, kaons, and protons show separate bands below 1 GeV/c and gradually merge at higher momenta. For a specific particle type i, the measured $\langle dE/dx \rangle$ can be described by the corresponding Bichsel function [62] $\langle dE/dx \rangle_i^{\mathrm{th}}$ (solid lines), and we select those candidates with $|n\sigma_i| < 2$, where

$$n\sigma_i = \frac{1}{\sigma_R} \ln\left(\frac{\langle dE/dx \rangle}{\langle dE/dx \rangle_i^{\mathrm{th}}}\right). \qquad (2)$$

Here, σ_R is the momentum-dependent $\langle dE/dx \rangle$ resolution. To improve the particle identification at higher momenta, the TOF detector is employed to deduce the mass squared of charged particles. The distribution of mass squared versus momentum in Fig. 4 (right) shows the separation between pions, kaons, and protons. To ensure the purity of identified particles, the upper bounds of momentum are set to be 2 GeV/c for protons and 1.6 GeV/c for pions and kaons, and the lower bounds of transverse momentum are 0.4 GeV/c for protons and 0.2 GeV/c for pions and kaons.

In practice, v_1 is measured with respect to the event plane (Ψ_{EP}), an estimated reaction plane, and corrected for its finite resolution ($R\{\Psi_{\mathrm{EP}}\}$) [31]:

$$v_1 = \langle \cos(\phi - \Psi_{\mathrm{EP}}) \rangle / R\{\Psi_{\mathrm{EP}}\}. \qquad (3)$$

The average is taken over all particles of interest in an event and then over all events. In collisions at $\sqrt{s_{NN}} = 200$ GeV, Ψ_{EP} is determined from the sideward deflection of spectator neutrons registered by the zero degree calorimeter shower-maximum detectors (ZDC-SMD, $|\eta| > 6.3$) [63], and $R\{\Psi_{\mathrm{EP}}\}$ is calculated using the correlation between the two ZDC-SMD event planes at forward and backward rapidities [31]. In Au + Au collisions at 27 GeV, the event plane detector (EPD, $|\eta| > 3.8$) [64] instead of the ZDC-SMD is used to estimate Ψ_{EP}, since the latter has a low efficiency. To account for the nonuniform EPD performance, we expand Eq. (3) into four terms:

$$v_1^{f,c} = \frac{1}{\langle \cos^2 \phi \rangle} \cdot \frac{\langle \cos \phi \cos \Psi^f \rangle}{\sqrt{2 \langle \cos \Psi^f \cos \Psi^b \rangle}}, \qquad (4)$$

$$v_1^{f,s} = \frac{1}{\langle \sin^2 \phi \rangle} \cdot \frac{\langle \sin \phi \sin \Psi^f \rangle}{\sqrt{2 \langle \sin \Psi^f \sin \Psi^b \rangle}}, \qquad (5)$$

$$v_1^{b,c} = \frac{1}{\langle \cos^2 \phi \rangle} \cdot \frac{\langle \cos \phi \cos \Psi^b \rangle}{\sqrt{2 \langle \cos \Psi^f \cos \Psi^b \rangle}}, \qquad (6)$$

$$v_1^{b,s} = \frac{1}{\langle \sin^2 \phi \rangle} \cdot \frac{\langle \sin \phi \sin \Psi^b \rangle}{\sqrt{2 \langle \sin \Psi^f \sin \Psi^b \rangle}}, \qquad (7)$$

where Ψ^f and Ψ^b are the event planes reconstructed at forward and backward rapidities, respectively. The $\langle \cos^2 \phi \rangle$ and $\langle \sin^2 \phi \rangle$ factors as a function of rapidity compensate for

TABLE I. The default and variation cuts in the estimation of systematic uncertainties for the v_1 analyses of Au + Au, Ru + Ru, and Zr + Zr events at $\sqrt{s_{NN}} = 200$ GeV and Au + Au at 27 GeV.

	Cuts	
Systems	Default	Variation
Au + Au 200 GeV	$-30 < V_{z,\mathrm{TPC}} < 30$ cm $N_{\mathrm{hits}} \geq 15$ DCA ≤ 2 cm	$-30 < V_{z,\mathrm{TPC}} < 0$ cm $N_{\mathrm{hits}} \geq 20$ DCA ≤ 1 cm
Ru + Ru and Zr + Zr 200 GeV	$-35 < V_{z,\mathrm{TPC}} < 25$ cm $N_{\mathrm{hits}} \geq 15$ DCA ≤ 3 cm	$-35 < V_{z,\mathrm{TPC}} < 0$ cm $N_{\mathrm{hits}} \geq 20$ DCA ≤ 2 cm
Au + Au 27 GeV	$-70 < V_{z,\mathrm{TPC}} < 70$ cm $N_{\mathrm{hits}} \geq 15$ DCA ≤ 2 cm	$-70 < V_{z,\mathrm{TPC}} < 0$ cm $N_{\mathrm{hits}} \geq 20$ DCA ≤ 1 cm

the detector acceptance effect, and they should be constantly $1/2$ for perfect detectors. The event planes from the ZDC-SMD and the EPD are further corrected to have uniform distributions with the method in Ref. [65]. The four terms in Eqs. (4)–(7) are averaged to give the final $v_1\{\mathrm{EPD}\}$ results. The event plane reconstructed from spectator nucleons registered by the ZDC-SMD and EPD detectors minimizes the nonflow contributions that are unrelated to the reaction plane orientation and arise from resonances, jets, strings, quantum statistics, and final-state interactions.

The systematic uncertainties of the v_1 measurements are assessed by varying each of the analysis cuts (as listed in Table I) within a reasonable range. We estimate the absolute difference ($|\Delta_i|$) between results with the default cut and with a particular cut variation. In addition, we also quote the absolute difference between the $v_1(\mathsf{y})$ slopes measured at forward and backward rapidities as a source of systematic uncertainty. For the analysis of protons, we examine the effect of protons emitted from the beam pipe in secondary interactions and find that it contributes less than 1% to the systematic error. The uncertainty due to the particle detection efficiency is found to be negligible. The final systematic error is the quadrature sum of the systematic errors from all the sources under consideration, each of which is calculated with $|\Delta_i|/\sqrt{12}$, assuming a uniform probability distribution.

III. RESULTS AND DISCUSSION

Figure 5 presents $v_1(\mathsf{y})$ for protons and antiprotons in Au + Au collisions at $\sqrt{s_{NN}} = 200$ GeV, isobar collisions at $\sqrt{s_{NN}} = 200$ GeV, and Au + Au collisions at $\sqrt{s_{NN}} = 27$ GeV in the centrality range of 50%–80%. Since the observed difference between the isobaric systems is very small (approximately 1σ difference), the Ru + Ru and Zr + Zr data are merged to increase statistics. In general, both protons and antiprotons have negative $dv_1/d\mathsf{y}$ values, mainly caused by the expansion of the tilted emission source [66] as demonstrated in Fig. 2. In Figs. 5(d)–5(f), we show the v_1 difference Δv_1 between protons and antiprotons as a function of rapidity. Linear fits (solid lines) that extrapolate to the origin are applied within $-0.8 < \mathsf{y} < 0.8$ and yield negative $d\Delta v_1/d\mathsf{y}$, with the significance levels of 5.2σ (5.4σ) in Au + Au (isobar) collisions at 200 GeV and 14.3σ in Au + Au at 27 GeV. Note that $\Delta(dv_1/d\mathsf{y})$ and $d\Delta v_1/d\mathsf{y}$ are equivalent to each other, and we stick to the notation $\Delta(dv_1/d\mathsf{y})$ in the following discussion. This is the first observation of significantly negative $\Delta(dv_1/d\mathsf{y})$ between protons and antiprotons in heavy-ion collisions and qualitatively agrees with the predictions of the aforementioned electromagnetic field effect, i.e., the dominance of the Faraday induction + Coulomb effect over the Hall and transported-quark effects. The more negative $\Delta(dv_1/d\mathsf{y})$ value at 27 GeV could be partially explained by the slower decay of the spectator-induced electromagnetic field at lower energies due to the longer passage time of incident nuclei. Moreover, the shorter lifetime of the QGP at lower energies causes a stronger remaining magnetic field at the time of chemical freeze-out [26]. At lower beam energies, antiprotons are more susceptible to annihilation in the baryon-rich environment. Nevertheless, the effect on antiproton v_1 should be marginal, since the antiproton flow measurements [40,55] still meet coalescence expectations.

Figure 6 shows the $\Delta(dv_1/d\mathsf{y})$ between positively and negatively charged hadrons [$\pi^{\pm}$, $K^{\pm}$, and $p(\bar{p})$] as a function of centrality in Au + Au (a) and isobar (b) collisions at $\sqrt{s_{NN}} = 200$ GeV and Au + Au collisions at $\sqrt{s_{NN}} = 27$ GeV (c). The $\Delta(dv_1/d\mathsf{y})$ values for each particle species are extracted with the same linear-function fit as in Fig. 5. For all the collision systems and energies, the proton results (closed crosses) display a decreasing trend: positive in central collisions and negative in peripheral ones. This sign change resembles the scenario speculated in Fig. 3(c). In central collisions, the magnetic field and the spectator

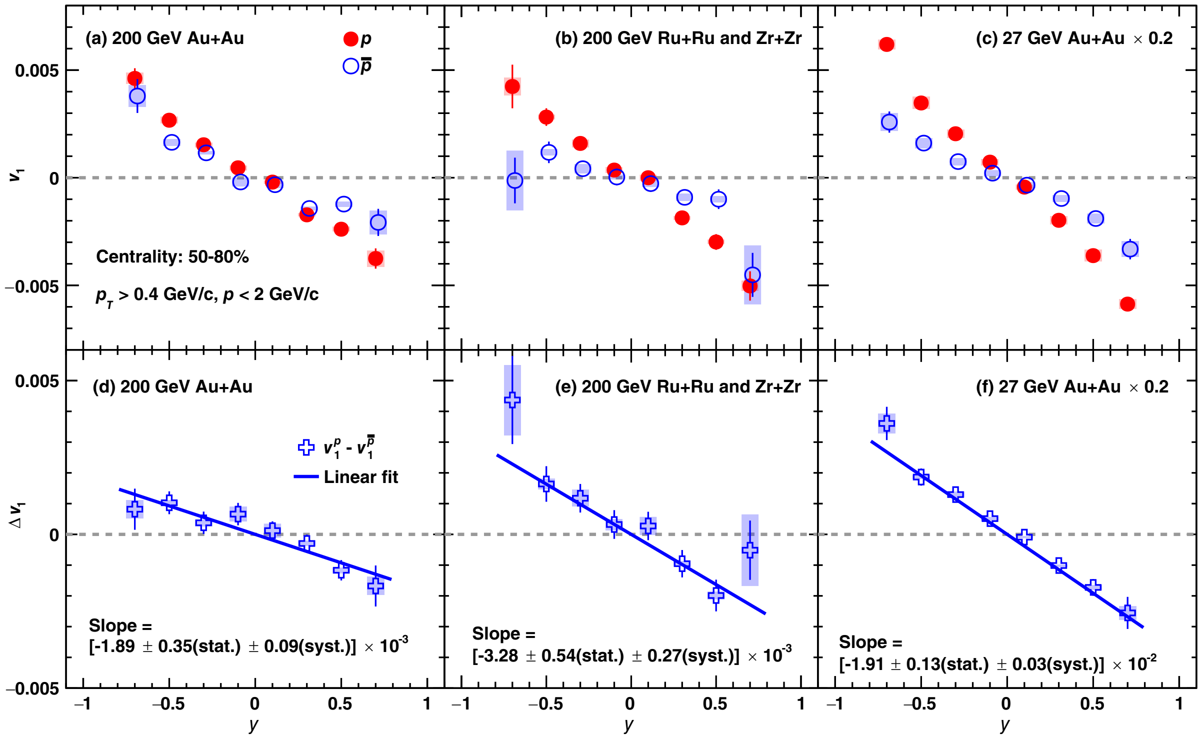

FIG. 5. v_1 for protons and antiprotons as a function of rapidity in (a) Au + Au collisions at $\sqrt{s_{NN}} = 200$ GeV, (b) isobar (Ru + Ru and Zr + Zr) collisions at $\sqrt{s_{NN}} = 200$ GeV, and (c) Au + Au collisions at $\sqrt{s_{NN}} = 27$ GeV in the centrality interval of 50%–80%. Protons and antiprotons are marked with solid and open circles, respectively. (d)–(f) show $\Delta v_1 \equiv v_1^p - v_1^{\bar{p}}$ versus rapidity. The $d\Delta v_1/dy$ values are obtained with linear fits (solid lines). Systematic uncertainties are indicated with shaded boxes.

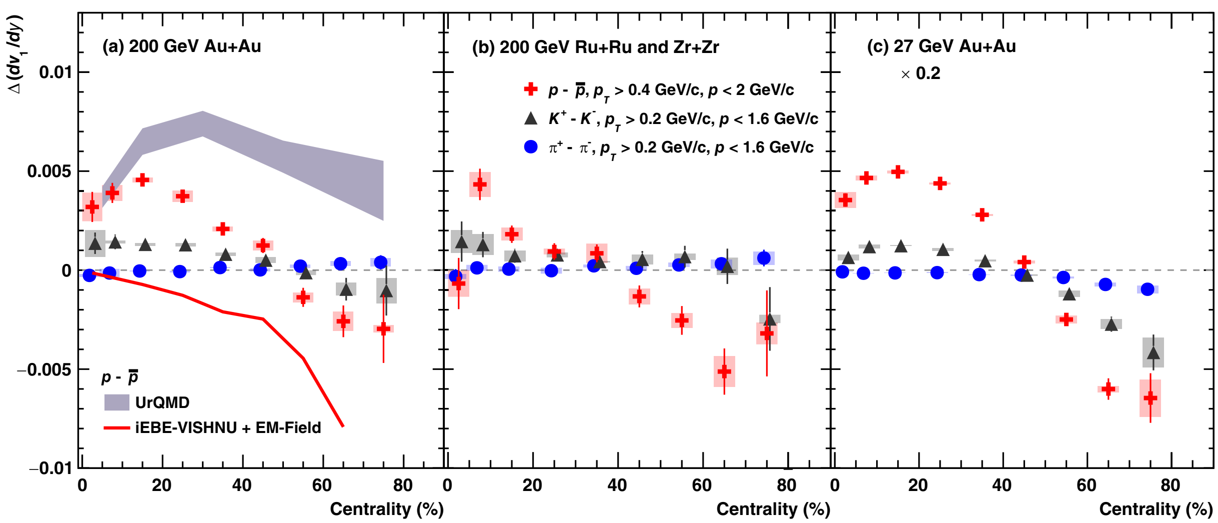

FIG. 6. $\Delta(dv_1/dy)$ between positively and negatively charged pions, kaons, and protons as a function of centrality in (a) Au + Au collisions at $\sqrt{s_{NN}} = 200$ GeV, (b) isobar collisions at $\sqrt{s_{NN}} = 200$ GeV, and (c) Au + Au collisions at $\sqrt{s_{NN}} = 27$ GeV. The lavender band indicates UrQMD simulations, without any EM-field effect, of the proton $\Delta dv_1/dy$ in Au + Au collisions at 200 GeV. In comparison, a solid curve is added correspondingly for the iEBE-VISHNU calculation with the electromagnetic field devoid of transported quarks [26].

Coulomb field are small, since there are few spectator protons, and the dominance of the transported-quark effect leads to the positive v_1 splitting. Toward more peripheral collisions, the electromagnetic field effect becomes stronger, keeps decreasing $\Delta(dv_1/dy)$, and finally changes the sign. The lavender band in Fig. 6(a) shows UrQMD simulations [67], which include no electromagnetic fields and give positive $\Delta(dv_1/dy)$ for protons due to transported-quark contributions. In Fig. 6(a), the solid curve gives the Event-By-Event Viscous Israel Stewart Hydrodynamics aNd UrQMD (iEBE-VISHNU) calculation of the electromagnetic-field contributions to the proton $\Delta(dv_1/d\mathrm{y})$ without transported quarks in Au + Au collisions at $\sqrt{s_{\mathrm{NN}}} = 200$ GeV [26]. The iEBE-VISHNU calculation adopts the electrical conductivity of the QGP at equilibrium, $\sigma = 0.023\ \mathrm{fm}^{-1}$, which is estimated from lattice QCD calculations [68–71] with a temperature of $T = 255$ MeV. Since transported quarks are generally believed to provide positive contributions to the proton $\Delta(dv_1/d\mathrm{y})$ [52–54], the negative $\Delta(dv_1/d\mathrm{y})$ values in peripheral events reveal the Faraday induction + Coulomb effect. In view of the potential interplay between transported quarks and the electromagnetic field, we abstain from simply adding these two models for a direct quantitative comparison with our data. However, it is noteworthy that the literal sum of the two model outcomes appears to align closely with the measurements, implying that the assumed electrical conductivity lies within a plausible interval.

The decreasing trend and the sign change of $\Delta(dv_1/d\mathrm{y})$ are also observed between K^+ and K^- (closed triangles) in Fig. 6, especially at 27 GeV. Kaons behave in a similar manner as protons, as only $K^+(u\bar{s})$ could be affected by transported u quarks. Quantitatively, we expect the $\Delta(dv_1/d\mathrm{y})$ for kaons to have a smaller magnitude than that for protons for several reasons. As shown in Fig. 4(right), kaons have lower mean momentum and, hence, lower mean p_T than protons, which can be translated into lower transported quark v_1 as well as weaker electromagnetic field effects [26]. On average, kaons also have a later formation time than protons due to their lighter mass, and the later-stage quark scatterings could reduce the existing v_1 splitting caused by the electromagnetic field. A factor that may complicate the interpretation of the kaon data is the potential asymmetry between s and $\bar{s}$ quarks. For example, the associated strangeness production $pp \to p\Lambda(1115)K^+$ [72] effectively converts net protons (the excess of p over $\bar{p}$) into $\Lambda(uds)$ and $K^+(u\bar{s})$, and, thus, K^+ receives additional contributions relative to K^-. Similar to the charm quarks, the $s(\bar{s})$ quarks are heavier and produced earlier than the $u(\bar{u})$ and $d(\bar{d})$ quarks and could be dominantly affected by the Hall effect, which reduces the splitting between K^+ and K^- in peripheral collisions.

The v_1 splitting between π^+ and π^- (closed circles) is less obvious than kaons and protons, but the pion $\Delta(dv_1/d\mathrm{y})$ is statistically significant, -0.0028 ± 0.0002, in 50%–80% Au + Au at 27 GeV. As mentioned before in the discussions related to Fig. 3, when transported quarks have positive $dv_1/d\mathrm{y}$, they should give negative contributions to the pion $\Delta(dv_1/d\mathrm{y})$. However, since π^+ and π^- are both affected by transported quarks, the net effect is much smaller than those for kaons and protons due to the cancellation. In a scenario where transported quarks have negative $dv_1/d\mathrm{y}$ [73], their contribution to the $\Delta(dv_1/d\mathrm{y})$ between π^+ and π^- should be positive, and then the negative pion $\Delta(dv_1/d\mathrm{y})$ values at 27 GeV support the dominance of the Faraday induction + Coulomb effect over the Hall effect. Therefore, the combined $\Delta(dv_1/d\mathrm{y})$ measurements for protons and pions favor the Faraday + Coulomb effect regardless of the sign of transported-quark v_1 in peripheral collisions. In principle, the electromagnetic effect should give rise to a negative $\Delta(dv_1/d\mathrm{y})$ between π^+ and π^- [26,74], but the aforementioned mechanisms, such as mean p_T and the formation time, are even more severe for pions than for kaons. The pions from neutral resonance decay may dilute the electromagnetic field effects, whereas the protons from Δ^{++} decay will enhance this effect, as Δ^{++} has two units of electric charge [26]. Therefore, the small magnitudes of the pion $\Delta(dv_1/d\mathrm{y})$ are understandable.

IV. CONCLUSION

The charge-dependent directed flow provides a probe to the transported quarks, as well as the Hall, Faraday, and Coulomb effects in heavy-ion collisions. We have presented the v_1 measurements for $\pi^{\pm}$, $K^{\pm}$, and $p(\bar{p})$ in Au + Au and isobar (Ru + Ru and Zr + Zr) collisions at $\sqrt{s_{\mathrm{NN}}} = 200$ GeV and Au + Au collisions at $\sqrt{s_{\mathrm{NN}}} = 27$ GeV. The slope difference $\Delta(dv_1/d\mathrm{y})$ between protons and antiprotons, as well as between K^+ and K^-, changes from positive values in central collisions to negative in peripheral collisions. The measured proton $\Delta(dv_1/d\mathrm{y})$ values in the centrality range of 50%–80% are $[-1.89 \pm 0.35(\mathrm{stat}) \pm 0.09(\mathrm{syst})] \times 10^{-3}$ in Au + Au collisions at 200 GeV, $[-3.28 \pm 0.53(\mathrm{stat}) \pm 0.27(\mathrm{syst})] \times 10^{-3}$ in isobar collisions at 200 GeV, and $[-1.91 \pm 0.13(\mathrm{stat}) \pm 0.03(\mathrm{syst})] \times 10^{-2}$ in Au + Au collisions at 27 GeV. While the positive $\Delta(dv_1/d\mathrm{y})$ for protons and kaons in central collisions can be attributed to the transported-quark contributions, the significant negative values in peripheral events are consistent with the electromagnetic field effects with the dominance of the Faraday induction + Coulomb effect [26–28]. The observed v_1 splitting for protons in Au + Au collisions at $\sqrt{s_{\mathrm{NN}}} = 200$ GeV is comparable in magnitude with the theoretical expectation incorporating both transported quarks [52–54] and the electromagnetic field [26]. The electrical conductivity of the QGP at equilibrium, $\sigma = 0.023\ \mathrm{fm}^{-1}$, given by lattice QCD calculations [68–71] with a temperature of $T = 255$ MeV, is found to be compatible with the measurements reported in this work. This charge splitting is stronger in collisions at $\sqrt{s_{\mathrm{NN}}} = 27$ GeV, corroborating the idea that the electromagnetic field decays more slowly at low energies. Compared with protons, pions and kaons have smaller $\Delta(dv_1/d\mathrm{y})$ magnitudes, which is understandable in view of factors such as mean p_T and the formation time. A companion STAR analysis [75] assumes the coalescence sum rule using combinations of hadrons without transported quarks and concludes that the presence of the

EM-field dominated by the Hall effect in midcentral events explains the observed v_1 splitting. The combined inference from Ref. [75] and the current work is that a competition between the Hall effect and the Faraday + Coulomb effect, its flavor, and centrality dependence may lead to the observed v_1 splittings. Further studies on the beam energy dependence of this observable are underway, with more data accumulated in the RHIC BES-II program.

ACKNOWLEDGMENTS

We thank the RHIC Operations Group and RCF at BNL, the NERSC Center at LBNL, and the Open Science Grid consortium for providing resources and support. This work was supported in part by the Office of Nuclear Physics within the U.S. DOE Office of Science, the U.S. National Science Foundation, National Natural Science Foundation of China, Chinese Academy of Science, the Ministry of Science and Technology of China and the Chinese Ministry of Education, the Higher Education Sprout Project by Ministry of Education at NCKU, the National Research Foundation of Korea, Czech Science Foundation and Ministry of Education, Youth and Sports of the Czech Republic, Hungarian National Research, Development and Innovation Office, New National Excellency Programme of the Hungarian Ministry of Human Capacities, Department of Atomic Energy and Department of Science and Technology of the Government of India, the National Science Centre and WUT ID-UB of Poland, the Ministry of Science, Education and Sports of the Republic of Croatia, German Bundesministerium für Bildung, Wissenschaft, Forschung and Technologie (BMBF), Helmholtz Association, Ministry of Education, Culture, Sports, Science, and Technology (MEXT), Japan Society for the Promotion of Science (JSPS), and Agencia Nacional de Investigación y Desarrollo (ANID) of Chile.

[1] E. Shuryak, *Strongly coupled quark-gluon plasma in heavy ion collisions*, Rev. Mod. Phys. **89**, 035001 (2017).

[2] E. W. Kolb and M. S. Turner, *The Early Universe*, Front. Phys. Vol. 69 (Westview Press, Boulder, 1990), p. 521.

[3] V. Voronyuk, V. D. Toneev, W. Cassing, E. L. Bratkovskaya, V. P. Konchakovski, and S. A. Voloshin, *(Electro-)magnetic field evolution in relativistic heavy-ion collisions*, Phys. Rev. C **83**, 054911 (2011).

[4] W.-T. Deng and X.-G. Huang, *Event-by-event generation of electromagnetic fields in heavy-ion collisions*, Phys. Rev. C **85**, 044907 (2012).

[5] X.-L. Zhao, G.-L. Ma, and Y.-G. Ma, *Impact of magnetic-field fluctuations on measurements of the chiral magnetic effect in collisions of isobaric nuclei*, Phys. Rev. C **99**, 034903 (2019).

[6] D. E. Kharzeev, L. D. McLerran, and H. J. Warringa, *The effects of topological charge change in heavy ion collisions: 'Event by event P and CP violation'*, Nucl. Phys. **A803**, 227 (2008).

[7] L. McLerran and V. Skokov, *Comments about the electromagnetic field in heavy-ion collisions*, Nucl. Phys. **A929**, 184 (2014).

[8] Z. Wang, J. Zhao, C. Greiner, Z. Xu, and P. Zhuang, *Incomplete electromagnetic response of hot QCD matter*, Phys. Rev. C **105**, L041901 (2022).

[9] C. Grayson, M. Formanek, J. Rafelski, and B. Muller, *Dynamic magnetic response of the quark-gluon plasma to electromagnetic fields*, Phys. Rev. D **106**, 014011 (2022).

[10] M. N. Chernodub, *Superconductivity of QCD vacuum in strong magnetic field*, Phys. Rev. D **82**, 085011 (2010).

[11] I. E. Frolov, V. C. Zhukovsky, and K. G. Klimenko, *Chiral density waves in quark matter within the Nambu-Jona-Lasinio model in an external magnetic field*, Phys. Rev. D **82**, 076002 (2010).

[12] M. N. Chernodub, *Spontaneous electromagnetic superconductivity of vacuum in strong magnetic field: Evidence from the Nambu-Jona-Lasinio model*, Phys. Rev. Lett. **106**, 142003 (2011).

[13] Y. Burnier, D. E. Kharzeev, J. Liao, and H.-U. Yee, *Chiral magnetic wave at finite baryon density and the electric quadrupole moment of quark-gluon plasma in heavy ion collisions*, Phys. Rev. Lett. **107**, 052303 (2011).

[14] X.-G. Huang, *Electromagnetic fields and anomalous transports in heavy-ion collisions—A pedagogical review*, Rep. Prog. Phys. **79**, 076302 (2016).

[15] K. Hattori and X.-G. Huang, *Novel quantum phenomena induced by strong magnetic fields in heavy-ion collisions*, Nucl. Sci. Tech. **28**, 26 (2017).

[16] D. E. Kharzeev and J. Liao, *Chiral magnetic effect reveals the topology of gauge fields in heavy-ion collisions*, Nat. Rev. Phys. **3**, 55 (2021).

[17] K. Fukushima, D. E. Kharzeev, and H. J. Warringa, *Chiral magnetic effect*, Phys. Rev. D **78**, 074033 (2008).

[18] D. E. Kharzeev, J. Liao, S. A. Voloshin, and G. Wang, *Chiral magnetic and vortical effects in high-energy nuclear collisions—A status report*, Prog. Part. Nucl. Phys. **88**, 1 (2016).

[19] V. P. Gusynin, V. A. Miransky, and I. A. Shovkovy, *Catalysis of dynamical flavor symmetry breaking by a magnetic field in $(2+1)$-dimensions*, Phys. Rev. Lett. **73**, 3499 (1994); **76**, 1005(E) (1996).

[20] K. Tuchin, *Synchrotron radiation by fast fermions in heavy-ion collisions*, Phys. Rev. C **82**, 034904 (2010); **83**, 039903 (E) (2011).

[21] A. J. Mizher, M. N. Chernodub, and E. S. Fraga, *Phase diagram of hot QCD in an external magnetic field: Possible splitting of deconfinement and chiral transitions*, Phys. Rev. D **82**, 105016 (2010).

[22] R. K. Mohapatra, P. S. Saumia, and A. M. Srivastava, *Enhancement of flow anisotropies due to magnetic field in relativistic heavy-ion collisions*, Mod. Phys. Lett. A **26**, 2477 (2011).

[23] K. Tuchin, *On viscous flow and azimuthal anisotropy of quark-gluon plasma in strong magnetic field*, J. Phys. G **39**, 025010 (2012).

[24] S. K. Das, S. Plumari, S. Chatterjee, J. Alam, F. Scardina, and V. Greco, *Directed flow of charm quarks as a witness of the initial strong magnetic field in ultra-relativistic heavy ion collisions*, Phys. Lett. B **768**, 260 (2017).

[25] A. Dubla, U. Gürsoy, and R. Snellings, *Charge-dependent flow as evidence of strong electromagnetic fields in heavy-ion collisions*, Mod. Phys. Lett. A **35**, 2050324 (2020).

[26] U. Gürsoy, D. Kharzeev, E. Marcus, K. Rajagopal, and C. Shen, *Charge-dependent flow induced by magnetic and electric fields in heavy ion collisions*, Phys. Rev. C **98**, 055201 (2018).

[27] U. Gursoy, D. Kharzeev, and K. Rajagopal, *Magnetohydrodynamics, charged currents and directed flow in heavy ion collisions*, Phys. Rev. C **89**, 054905 (2014).

[28] K. Nakamura, T. Miyoshi, C. Nonaka, and H. R. Takahashi, *Charge-dependent anisotropic flow in high-energy heavy-ion collisions from a relativistic resistive magneto-hydrodynamic expansion*, Phys. Rev. C **107**, 034912 (2023).

[29] L. Adamczyk *et al.* (STAR Collaboration), *Charge-dependent directed flow in* Cu + Au *collisions at* $\sqrt{s_{NN}} = 200$ GeV, Phys. Rev. Lett. **118**, 012301 (2017).

[30] L. Adamczyk *et al.* (STAR Collaboration), *Azimuthal anisotropy in* Cu + Au *collisions at* $\sqrt{s_{NN}} = 200$ GeV, Phys. Rev. C **98**, 014915 (2018).

[31] A. M. Poskanzer and S. A. Voloshin, *Methods for analyzing anisotropic flow in relativistic nuclear collisions*, Phys. Rev. C **58**, 1671 (1998).

[32] S. A. Voloshin and T. Niida, *Ultrarelativistic nuclear collisions: Direction of spectator flow*, Phys. Rev. C **94**, 021901(R) (2016).

[33] M. Luzum and J.-Y. Ollitrault, *Directed flow at midrapidity in heavy-ion collisions*, Phys. Rev. Lett. **106**, 102301 (2011).

[34] U. Heinz and R. Snellings, *Collective flow and viscosity in relativistic heavy-ion collisions*, Annu. Rev. Nucl. Part. Sci. **63**, 123 (2013).

[35] J. Adams *et al.* (STAR Collaboration), *Directed flow in* Au + Au *collisions at* $\sqrt{s_{NN}} = 62.4$ GeV, Phys. Rev. C **73**, 034903 (2006).

[36] B. I. Abelev *et al.* (STAR Collaboration), *System-size independence of directed flow at the Relativistic Heavy-Ion Collider*, Phys. Rev. Lett. **101**, 252301 (2008).

[37] G. Agakishiev *et al.* (STAR Collaboration), *Directed and elliptic flow of charged particles in* Cu + Cu *collisions at* $\sqrt{s_{NN}} = 22.4$ GeV, Phys. Rev. C **85**, 014901 (2012).

[38] L. Adamczyk *et al.* (STAR Collaboration), *Directed flow of identified particles in* Au + Au *collisions at* $\sqrt{s_{NN}} =$ 200 GeV *at RHIC*, Phys. Rev. Lett. **108**, 202301 (2012).

[39] L. Adamczyk *et al.* (STAR Collaboration), *Beam-energy dependence of the directed flow of protons, antiprotons, and pions in* Au + Au *collisions*, Phys. Rev. Lett. **112**, 162301 (2014).

[40] L. Adamczyk *et al.* (STAR Collaboration), Beam-energy dependence of directed flow of Λ, $\bar{\Lambda}$, $K^{\pm}$, K_s^0 and ϕ in Au + Au collisions, Phys. Rev. Lett. **120**, 062301 (2018).

[41] J. Adam *et al.* (STAR Collaboration), *First observation of the directed flow of* D^0 *and* $\overline{D^0}$ *in* Au + Au *collisions at* $\sqrt{s_{\rm NN}} = 200$ GeV, Phys. Rev. Lett. **123**, 162301 (2019).

[42] J. Adam *et al.* (STAR Collaboration), *Beam-energy dependence of the directed flow of deuterons in* Au + Au *collisions*, Phys. Rev. C **102**, 044906 (2020).

[43] B. Abelev *et al.* (ALICE Collaboration), *Directed flow of charged particles at midrapidity relative to the spectator plane in* Pb – Pb *collisions at* $\sqrt{s_{NN}} = 2.76$ TeV, Phys. Rev. Lett. **111**, 232302 (2013).

[44] In our notation, $\Delta(dv_1/d\mathrm{y})$ is the $dv_1/d\mathrm{y}$ difference between positively charged particles and their negatively charged antiparticles. For example, proton $\Delta(dv_1/d\mathrm{y})$ means the $dv_1/d\mathrm{y}$ difference between protons and antiprotons.

[45] D. Molnar and S. A. Voloshin, *Elliptic flow at large transverse momenta from quark coalescence*, Phys. Rev. Lett. **91**, 092301 (2003).

[46] J. C. Dunlop, M. A. Lisa, and P. Sorensen, *Constituent quark scaling violation due to baryon number transport*, Phys. Rev. C **84**, 044914 (2011).

[47] A. Goudarzi, G. Wang, and H. Z. Huang, *Evidence of coalescence sum rule in elliptic flow of identified particles in high-energy heavy-ion collisions*, Phys. Lett. B **811**, 135974 (2020).

[48] R. C. Hwa and C. B. Yang, *Scaling distributions of quarks, mesons, and proton for all* p_T*, energy, and centrality*, Phys. Rev. C **67**, 064902 (2003).

[49] R. J. Fries, B. Müller, C. Nonaka, and S. A. Bass, *Hadronization in heavy-ion collisions: Recombination and fragmentation of partons*, Phys. Rev. Lett. **90**, 202303 (2003).

[50] V. Greco, C. M. Ko, and P. Lévai, *Parton coalescence and the antiproton/pion anomaly at RHIC*, Phys. Rev. Lett. **90**, 202302 (2003).

[51] S. Acharya *et al.* (ALICE Collaboration), *Probing the effects of strong electromagnetic fields with charge-dependent directed flow in* Pb – Pb *collisions at the LHC*, Phys. Rev. Lett. **125**, 022301 (2020).

[52] Y. Guo, F. Liu, and A. Tang, *Directed flow of transported and non-transported protons in* Au + Au *collisions from UrQMD model*, Phys. Rev. C **86**, 044901 (2012).

[53] K. Nayak, S. Shi, N. Xu, and Z.-W. Lin, *Energy dependence study of directed flow in* Au + Au *collisions using an improved coalescence in a multiphase transport model*, Phys. Rev. C **100**, 054903 (2019).

[54] P. Bozek, *Splitting of proton-antiproton directed flow in relativistic heavy-ion collisions*, Phys. Rev. C **106**, L061901 (2022).

[55] L. Adamczyk *et al.* (STAR Collaboration), *Centrality dependence of identified particle elliptic flow in relativistic heavy ion collisions at* $\sqrt{s_{NN}} =$ 7.7–62.4 GeV, Phys. Rev. C **93**, 014907 (2016).

[56] M. Anderson *et al.*, *The STAR time projection chamber: A unique tool for studying high multiplicity events at RHIC*, Nucl. Instrum. Methods Phys. Res., Sect. A **499**, 659 (2003).

[57] W. Llope *et al.*, *The STAR vertex position detector*, Nucl. Instrum. Methods Phys. Res., Sect. A **759**, 23 (2014).

[58] M. L. Miller, K. Reygers, S. J. Sanders, and P. Steinberg, *Glauber modeling in high energy nuclear collisions*, Annu. Rev. Nucl. Part. Sci. **57**, 205 (2007).

[59] B. I. Abelev *et al.* (STAR Collaboration), *Systematic measurements of identified particle spectra in* pp, d^{+} Au *and* Au + Au *collisions from STAR*, Phys. Rev. C **79**, 034909 (2009).

[60] M. Abdallah *et al.* (STAR Collaboration), *Search for the chiral magnetic effect with isobar collisions at* $\sqrt{s_{NN}} =$ 200 GeV *by the STAR Collaboration at the BNL Relativistic Heavy Ion Collider*, Phys. Rev. C **105**, 014901 (2022).

[61] W. Llope *et al.*, *The TOFp/pVPD time-of-flight system for star*, Nucl. Instrum. Methods Phys. Res., Sect. A **522**, 252 (2004).

[62] H. Bichsel, *A method to improve tracking and particle identification in TPCs and silicon detectors*, Nucl. Instrum. Methods Phys. Res., Sect. A **562**, 154 (2006).

[63] C. Adler, A. Denisov, E. Garcia, M. Murray, H. Stroebele, and S. White, *The RHIC zero degree calorimeters*, Nucl. Instrum. Methods Phys. Res., Sect. A **470**, 488 (2001).

[64] J. Adams *et al.*, *The STAR event plane detector*, Nucl. Instrum. Methods Phys. Res., Sect. A **968**, 163970 (2020).

[65] J. Barrette *et al.* (E877 Collaboration), *Proton and pion production relative to the reaction plane in* $\mathrm{Au}+\mathrm{Au}$ *collisions at* 11 GeV/c, Phys. Rev. C **56**, 3254 (1997).

[66] J. Brachmann, S. Soff, A. Dumitru, H. Stöcker, J. A. Maruhn, W. Greiner, L. V. Bravina, and D. H. Rischke, *Antiflow of nucleons at the softest point of the equation of state*, Phys. Rev. C **61**, 024909 (2000).

[67] S. A. Bass *et al.*, *Microscopic models for ultrarelativistic heavy ion collisions*, Prog. Part. Nucl. Phys. **41**, 255 (1998).

[68] H. T. Ding, A. Francis, O. Kaczmarek, F. Karsch, E. Laermann, and W. Soeldner, *Thermal dilepton rate and electrical conductivity: An analysis of vector current correlation functions in quenched lattice QCD*, Phys. Rev. D **83**, 034504 (2011).

[69] A. Francis and O. Kaczmarek, *On the temperature dependence of the electrical conductivity in hot quenched lattice QCD*, Prog. Part. Nucl. Phys. **67**, 212 (2012).

[70] B. B. Brandt, A. Francis, H. B. Meyer, and H. Wittig, *Thermal correlators in the* ρ *channel of two-flavor QCD*, J. High Energy Phys. 3 (2013) 001.

[71] A. Amato, G. Aarts, C. Allton, P. Giudice, S. Hands, and J.-I. Skullerud, *Electrical conductivity of the quark-gluon plasma across the deconfinement transition*, Phys. Rev. Lett. **111**, 172001 (2013).

[72] J. Balewski *et al.*, *Total cross section of the reaction* $pp \to pK^+\Lambda$ *close to threshold*, Phys. Lett. B **420**, 211 (1998).

[73] T. Parida and S. Chatterjee, *Baryon inhomogeneities driven charge dependent directed flow in heavy ion collisions*, arXiv:2305.08806.

[74] J.-J. Zhang, X.-L. Sheng, S. Pu, J.-N. Chen, G.-L. Peng, J.-G. Wang, and Q. Wang, *Charge-dependent directed flows in heavy-ion collisions by Boltzmann-Maxwell equations*, Phys. Rev. Res. **4**, 033138 (2022).

[75] STAR Collaboration, *Electric charge and strangeness-dependent directed flow splitting of produced quarks in* $\mathrm{Au}+\mathrm{Au}$ *collisions*, arXiv:2304.02831.